Electronic-Raman-scattering study of the low-lying energy levels of trivalent cerium-doped yttria

G. S. Nolas,* V. G. Tsoukala,† and S. K. Gayen
Department of Physics and Engineering Physics, Stevens Institute of Technology, Hoboken, New Jersey 07030

Glen A. Slack*
General Electric Research and Development Center, Schenectady, New York 12301
(Received 24 September 1993; revised manuscript received 16 March 1994)

Electronic-Raman (ER) transitions from the ground level of the $^2F_{5/2}$ manifold to other $4f$ levels of trivalent cerium (Ce^{3+}) in yttria (Y_2O_3) have been studied as a function of excitation wavelength and temperature. ER transitions were observed for Ce^{3+} occupying both the C_{3i} and C_2 sites in Y_2O_3. Energy-level positions of the Kramer doublets of Ce^{3+} in the C_{3i} site were determined from this measurement. The levels of the $^2F_{5/2}$ manifold were at 978 and 1503 cm^{-1}, while three of the four levels of the $^2F_{7/2}$ manifold were at 2270, 2996, and 3402 cm^{-1} above the ground level. Previous literature values of three of the four energy levels of the $^2F_{7/2}$ manifold of the C_2 site were confirmed. A level of the $^2F_{5/2}$ manifold of Ce^{3+} in the C_2 site at 666 cm^{-1} was also identified. For resonant excitation involving a $5d$ intermediate state, two-orders-of-magnitude enhancement in the ER transition strength was observed. This resonant enhancement effect makes the electronic-Raman-scattering technique site selective, since for resonant excitation of the intermediate state of a particular site the ER lines of that site become more intense than those belonging to the other site. The differential scattering cross section for the transition from the ground state to the lowest $^2F_{7/2}$ level was measured to be 2.2×10^{-30} $cm^2\,sr^{-1}\,ion^{-1}$ for the C_2 site, and 8.8×10^{-30} $cm^2\,sr^{-1}\,ion^{-1}$ for the C_{3i} site. These experimental values of cross sections are compared to the theoretical estimates.

I. INTRODUCTION

The results of an electronic-Raman-scattering (ERS) study of the energy-level structure of the trivalent cerium ion (Ce^{3+}) doped into yttria (Y_2O_3) are presented in this paper. ERS is an inelastic light-scattering process whereby an incident photon interacts with a material system (atom, ion, or molecule) and a second photon is emitted while the system makes a transition to an electronic state higher (Stokes ERS) or lower (anti-Stokes ERS) in energy than the initial state. The energy of the final state is the difference in energy between incident and scattered photons. A variety of systems including rare-earth and transition-metal ion-doped crystals and glasses, diatomic molecules, and metallocene complexes have been investigated by ERS.[1] Interest in ERS is primarily in the determination of the symmetry and energy of low-lying levels of these systems.

The study of ERS in rare-earth crystals was initiated by Hougen and Singh,[2,3] who studied trivalent praseodymium (Pr^{3+}) in $PrCl_3$ following the theoretical prediction of Elliot and Loudon.[4] Chau[5] then observed ERS of trivalent cerium (Ce^{3+}) in $CaWO_4$. These experiments were performed with a mercury arc as the excitation source and the Raman-scattered light recorded on photographic plates. Köningstein and co-workers used laser-excited ERS to study various trivalent rare-earth (R^{3+}) ions in garnet, chloride, vanadate, and aluminate hosts.[1,6,7] They used the technique to extract crystal-field parameters, to determine energy-level positions and assign their symmetry, to investigate the Zeeman splitting of Kramer doublets, to study the temperature dependence of magnetic susceptibility, and to demonstrate resonance enhancement effects. They also investigated epitaxial thin films of rare-earth-doped garnets.

Electronic-Raman scattering has been used in the study of most of the rare-earth ions in a number of host crystals. To the best of our knowledge, the rare-earth ions studied so far are Ce^{2+},[1] Sm^{2+},[8] Ce^{3+},[1,5,9–11] Nd^{3+},[1] Eu^{3+},[1,12] Tb^{3+},[1] Er^{3+},[1,12,13] and Yb^{3+}.[1] The rare-earth ions studied using ERS for which the ion was a stochiometric constituent of the crystal are Sm^{2+},[8] Ce^{3+},[1,14–17] Pr^{3+},[1,3,18] Nd^{3+},[1,19] Sm^{3+},[1] Eu^{3+},[1] Tb^{3+},[1,20,21] Dy^{3+},[1,22] Er^{3+},[1,12,13,22–24] Tm^{3+},[1,23,25,26] and Yb^{3+}.[1,12,22,25]

Trivalent cerium is perhaps the most well studied R^{3+} ion using the ERS technique.[1,5,9–11,14–17] In the present study we concentrate on the Ce^{3+}:Y_2O_3 system, which is interesting for several reasons. First, Ce^{3+} substitutes for Y^{3+} in Y_2O_3 in two inequivalent sites with C_2 and C_{3i} local symmetry. However, the energy-level structures of these two different centers have not yet been fully established. The system is at best weakly fluorescing,[27] which complicates the study of low-lying energy levels by fluorescence spectroscopy. On the basis of infrared-absorption measurements, Chang *et al.*[28] determined the positions of the energy levels of the $^2F_{7/2}$ manifold of the C_2 site, but those of the C_{3i} site had not been studied. Since Raman scattering is a two-photon process that connects states of the same symmetry and thus complements ir measurements, it is expected that ERS measurements will help establish the energy-level structure of the low-lying states of the C_{3i} site. Second, the site selectivity of the ERS technique may be tested in this system, which is

expected to elucidate the strength of the technique itself. Third, Ce^{3+} has a single optically active electron, which leads to a simpler energy-level structure compared to that of other R^{3+} ions, making analysis of ERS data easier. Also, the strong crystal-field interaction of the yttria host positions the lowest Ce^{3+} $5d$ level of the two sites in the blue-green spectral region, which is easily accessible to radiation from light sources commonly used for Raman studies. By tuning in and out of a resonance of a particular site, one may examine the resonant enhancement of the electronic-Raman (ER) transition strength. Resonance enhancement enables one to study Raman lines which are weak for nonresonant excitation. It also helps to identify the ER transitions within the states of a particular site, since resonant excitation leads to a preferential enhancement of Raman lines originating from that site.

This paper is organized in several sections. In Sec. II the crystal structure and site occupation of Ce^{3+} in Y_2O_3 is presented, and results of linear spectroscopy of Ce^{3+}:Y_2O_3 are discussed. Section III outlines the experimental procedure and parameters for ERS measurements. Section IV contains the experimental results. The measured ERS cross sections are compared to those for Ce^{3+} in other hosts in the literature. In Sec. V a simple theoretical argument is provided which gives a qualitative comparison of the ERS cross sections obtained experimentally. The conclusions of this study are summarized in Sec. VI.

II. SAMPLE CHARACTERISTICS, CRYSTAL STRUCTURE, AND LINEAR SPECTROSCOPY

The samples used in the ERS experiments were polycrystalline Ce^{3+}:Y_2O_3, Eu^{3+}:Y_2O_3, and undoped Y_2O_3 sintered plates, pressed to high density, nearly free of porosity, and semitransparent, made from fine powders by a process developed by Dibianca *et al.*[29] The ERS spectra of Eu^{3+}-doped Y_2O_3 and undoped Y_2O_3 samples were used in order to compare these with those of Ce^{3+}-doped Y_2O_3. This helps distinguish the contributions of scattering from Ce^{3+} centers. The thin-disk Ce^{3+}:Y_2O_3 sample had approximate dimensions of $10\times5\times0.5$ mm^3. All samples had a similar thickness of ~0.5 mm. Cerium-doped samples had been annealed at 1800 °C in a low partial pressure of oxygen such that almost all of the rare-earth ions present were trivalent and practically none were tetravalent.[30] The cerium concentration in the Ce^{3+}:Y_2O_3 sintered plate was 1 mol %, which is equivalent to an ion density of 2.68×10^{20} cm^{-3}.

Yttrium oxide (Y_2O_3) crystallizes into the cubic C-type rare-earth oxide (bixbyite) structure with space group T_h^7 ($Ia3$).[31] The elementary cell contains 16 formula units with 32 cations distributed in C_2 and C_{3i} sites in a 3:1 ratio.[32] Electron paramagnetic resonance studies[33] have demonstrated that Ce^{3+} may enter substitutionally for Y^{3+} in both C_{3i} and C_2 sites. The relative populations in the two sites were not determined. However, on the basis of site occupation probability of Eu^{3+} in Y_2O_3 as well as in isostructural Sc_2O_3 and Lu_2O_3 as determined by absorption[34] and Mössbauer[35] measurements, it is presumed that Ce^{3+} ions occupy both the sites with equal probability.

The room-temperature absorption spectrum of the Ce^{3+}:Y_2O_3 transparent sintered plate from 190 to 700 nm, taken with a Perkin-Elmer Lambda-9 uv-visible–near-infrared spectrophotometer, is displayed in Fig. 1. The spectrum is characterized by two broad bands centered at 440 and 250 nm. At room temperature the two bands partially overlap, but are resolved. These absorption bands are due to electric-dipole transitions from the $^2F_{5/2}$ state of the $4f$ ground configuration to states of the $5d$ configuration of the Ce^{3+} ion in both C_{3i} and C_2 sites. The onset of the fundamental absorption edge of Y_2O_3 occurs at 220 nm.[36] The higher-energy band is therefore an overlap of both Ce^{3+} absorption and absorption by the host crystal.

The contributions of absorptive transitions within the states of C_{3i} and C_2 sites to the overall absorption spectrum may not be readily separated out from the structureless bands displayed in Fig. 1. The relatively large optical thickness of our sample did not allow for the resolution of the $5d$ bands in the absorption spectrum. Diffuse reflectance spectra of a powder sample of 1% Ce^{3+} in Y_2O_3, taken with a Hitachi model U-3410 spectrophotometer, however, showed broad overlapping but distinct structures with maxima centered at approximately 19 400 cm^{-1} (516 nm) and 22 700 cm^{-1} (441 nm), due to transitions to the lowest excited $5d$ level of Ce^{3+} in C_{3i} and C_2 sites, respectively.[30]

The Ce^{3+}:Y_2O_3 system is very weakly fluorescing. Blasse and Brill reported two fluorescence peaks at 19 600 cm^{-1} (510 nm) and 24 000 cm^{-1} (417 nm) for short-

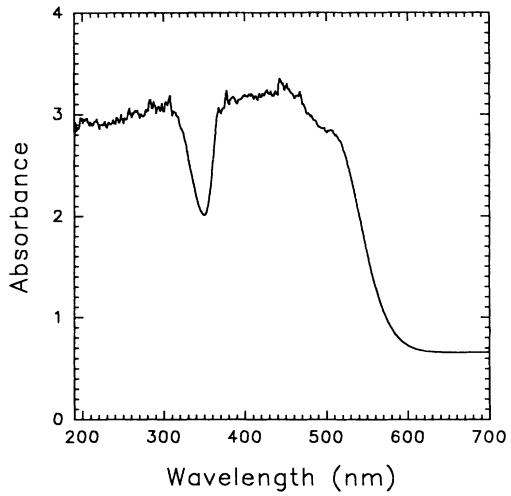

FIG. 1. Absorption spectrum of 1% Ce^{3+}:Y_2O_3 at room temperature covering the 190–700 nm spectral region. No absorption was observed in the range 700–3200 nm except for a small peak at 2620 nm, which was due to a transition to the highest-energy level of the $^2F_{7/2}$ manifold of Ce^{3+} in the C_2 site. The sintered-plate sample had dimensions of $10\times5\times0.5$ mm^3. The absorption measurements were taken along the 0.5-mm path length of the sample. The small, sharp structures at the absorbance maximum of the figure are instrumental noise and not due to Ce^{3+}.

wavelength uv excitation.[27] Exciting with the 514.5- and 488-nm Ar^+-laser lines, we observed a broad band extending from approximately 590 to 880 nm with the peak at 735 nm and a linewidth [full width at half maximum (FWHM)] of 3190 cm^{-1}. Exciting with 7-ns, 532-nm pulses from a Nd:YAG laser (Quanta Ray DCR-3G) and using a fast detector and oscilloscope (Tektronix model 11201 digitizing oscilloscope), we measured a room-temperature fluorescence lifetime of ~ 10 ns, which is somewhat shorter but of the same order of magnitude as a typical Ce^{3+} fluorescence lifetime in other hosts.[37]

The lower-lying states belonging to the $4f$ configuration of Ce^{3+} in C_2 sites were observed by Chang *et al.*[28] Employing infrared absorption measurements, they determined the positions of the Stark levels of the $^2F_{7/2}$ manifold to be at 2182, 2750, 3061, and 3880 cm^{-1} at a temperature of 80 K. In the present study, we have complemented our ERS spectra with ir-absorption spectra. Measurements on the sintered plate taken with Nicolet models 740 and 7199 Fourier-transform-infrared (FTIR) spectrometers helped identify three of the four energy levels of the $^2F_{7/2}$ manifold of the C_2 site at 2127, 2785, and 3825 cm^{-1} and the lowest level of the $^2F_{7/2}$ manifold of the C_{3i} site at 2264 cm^{-1} at room temperature. The linewidths obtained from our ir-absorption spectra[30] ranged from 2.9 to 30 cm^{-1}.

III. EXPERIMENTAL ARRANGEMENT

Most of the ERS spectra used in this study were measured with a backscattering geometry. Excitation sources included an Ar^+ laser (514.5, 501.7, 488, 476.5, and 457.9 nm lines) and a He-Ne laser (632.8 nm). The laser light was focused onto the sample using a 10-cm-focal-length cylindrical lens.

A half-wave plate rotated the polarization of the laser beam. The maximum Raman signal was obtained for an angle of incidence of 60°. The Brewster's angle is 63° for this sample. The scattered light was collected by an $f/2$ lens and focused by a 307-mm-focal-length lens onto the entrance slit of a double monochromator (Spex Industries model 1401) equipped with 1200-lines/mm gratings blazed at 500 nm. The dispersed light at the exit slit of the double monochromator was detected by a cooled photomultiplier tube (Burle C31034) with an S-20 spectral response. In order to detect the intrinsically weak ERS signal with adequate sensitivity, the output signal from the photomultiplier tube was amplified by a preamplifier (Stanford Research Systems model SR445) and processed by a photon counter (Stanford Research Systems model SR400) interfaced to a personal computer. The spectral resolution used in obtaining the ERS spectra varied from 1.0 to 3.5 cm^{-1} for different runs. The 992-cm^{-1} vibrational mode of benzene was used in the daily frequency calibration of the Raman system. In addition, the 379-cm^{-1} $A_g + T_g$ vibrational mode[38] of Y_2O_3 was used as a reference to obtain the frequency shift of the ER lines.

Low-temperature measurements were taken by mounting the samples on a cold finger in the tail section of a cryostat, which used a pool of liquid nitrogen to cool the sample by conduction. A copper-Constantan thermocouple measured the temperature of the cold finger near the sample to be 92 K with a maximum variation of ~ 0.25 K per run.

IV. EXPERIMENTAL RESULTS

A. Electronic-Raman scattering spectra

The Stokes electronic-Raman spectrum of Ce^{3+}:Y_2O_3 taken at a sample temperature of 92 K is displayed in Fig. 2. The spectrum which covers a frequency-shift range of 600–3900 cm^{-1} from the excitation frequency is highly structured. A number of sharp lines appear between 600 and 2500 cm^{-1} from the excitation frequency. Beyond 2500 cm^{-1} there are fewer sharp lines on a slowly rising background. The sharp lines in the spectrum originate from two different types of transitions: (a) intra-$4f$ electronic-Raman transitions in Ce^{3+} and (b) fluorescence of Eu^{3+} and Pr^{3+} which may have been present in trace amounts in the starting material used for making the sample. The rising background is the beginning of the Ce^{3+} fluorescence discussed in Sec. II. The ERS lines arising from transitions within the $4f$ levels of both the C_{3i} and C_2 sites of Ce^{3+} are denoted by arrows in Fig. 2. The peak positions, linewidths (FWHM), and integrated intensities of the ER transitions at a temperature of 92 K are listed in Table I. The assignment of transitions to either C_{3i} or C_2 sites was facilitated by site selectivity of resonance enhancement, to be discussed later in this section. The value in italics in Table I is for a C_2-site ER transition too weak to be observed with the 514.5 nm excitation and does not appear in the spectrum of Fig. 2. The intensity of this ER transition was strongest for 457.9 nm excitation.

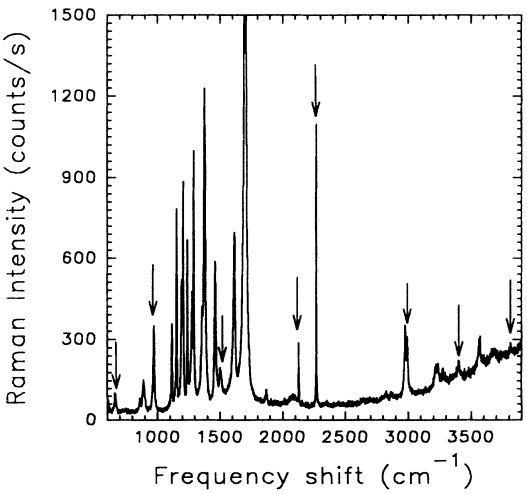

FIG. 2. Stokes ERS spectrum of 1% Ce^{3+}:Y_2O_3 at a sample temperature of 92 K for 514.5 nm excitation. Arrows indicate the ER transitions within the states of Ce^{3+}. The other features were due to Eu^{3+} and Pr^{3+} fluorescence, as described in the text. The vibrational modes of the host lattice lie below 610 cm^{-1} and are now shown in the spectrum. The frequency resolution in this measurement was ~ 2 cm^{-1}.

TABLE I. Frequency shift, linewidth, and intensity of the observed Stokes ER transitions of the $4f^1$ ground configuration of Ce^{3+} in Y_2O_3 from ERS measurements using 514.5 nm excitation at a temperature of 92 K. The values written in italics are for 457.9 nm excitation. Levels not observed by ERS are indicated by dashes. The intensities were normalized by the intensity of the 379-cm^{-1} vibrational mode of Y_2O_3.

Site	Multiplet	Frequency shift (cm^{-1})	Linewidth (cm^{-1})	Normalized intensity
C_2	$^2F_{5/2}$	666	10.0	0.155
		—	—	—
	$^2F_{7/2}$	2129	3.0	0.375
		2793	*8.0*	*0.225*
		—	—	—
		3814	8.0	0.020
C_{3i}	$^2F_{5/2}$	978	6.0	0.609
		1503	15.0	0.268
	$^2F_{7/2}$	2270	3.5	1.215
		2996	8.0	0.915
		3402	8.0	0.155
		—	—	—

The linewidths of the ER transitions decreased and the peak intensities increased as the temperature was decreased from room temperature to 92 K. In addition, small shifts ranging from 1 to 27 cm^{-1} in the position of the ER lines were observed at low temperature as compared to the room-temperature positions. The positions of energy levels at 92 K and room temperature are compared in Table II. Energy-level positions determined from infrared-absorption measurements[28,30] are also presented in the table. The difference in energy-level positions obtained from our measurements to those of Chang *et al.*[28] may be attributed to the polycrystalline nature of our sample, while single crystals were used in the other measurement. However, since no spectra or linewidths were given by Chang *et al.*,[28] the accuracy of their level positions is difficult to assess. Within a given manifold, the linewidth increased for transitions terminating on higher-lying levels. This is a consequence of lifetime broadening of the higher levels, which readily decay by phonon emission.

Several tests were used to distinguish the ERS lines from other contributions mentioned above. First, Stokes ERS spectra were taken with different excitation frequencies. The frequency shift of the ERS lines (indicated by arrows in Fig. 2) did not change, within experimental tolerance, for different excitation frequencies, while the relative position of the fluorescence lines changed. In addition, spectra of undoped Y_2O_3 and Eu^{3+}:Y_2O_3 were measured at 514.5 and 488 nm excitations in order to compare with those of Ce^{3+}:Y_2O_3. No structure was observed in the spectra of undoped Y_2O_3 with frequency shifts corresponding to those indicated by arrows in Fig. 2. However, the sharp features in Fig. 2 not indicated by an arrow in the range 850–2500 cm^{-1} were observed in spectra of Eu^{3+}:Y_2O_3 with over two-orders-of-magnitude higher intensity. The absolute frequency (not the frequency shift) of these features did not change for 514.5 and 488 nm laser excitation. This indicates that these features were due to Eu^{3+} fluorescence. Similarly, features not indicated by arrows in Fig. 2 above 2500 cm^{-1} are presumed to be due to Pr^{3+} transitions. Further analysis of both the Ce^{3+}-doped and undoped samples revealed the unwanted impurity ion concentration to vary from 0.001% to 0.003%. However, fluorescence being a linear optical process may give rise to as much as a three-orders-of-magnitude intense signal than the nonlinear ERS process.[1] So even with approximately three-

TABLE II. Comparison of energy-level positions of the $4f^1$ configuration of Ce^{3+}:Y_2O_3 as determined by the ERS technique to those obtained from ir-absorption measurements. The parentheses denote calculated values.

		Energy (cm^{-1}) determined by			
		electronic-Raman scattering at		ir absorption at	
Site	Multiplets	92 K[a]	300 K[a]	80 K[b]	300 K[c]
C_2	$^2F_{5/2}$	666	659	(653)	—
		—	—	(1130)	—
	$^2F_{7/2}$	2129	2134	2182	2127
		2793	2766	2750	2785
		—	—	3061	—
		3814	3828	3880	3825
C_{3i}	$^2F_{5/2}$	978	969	—	—
		1503	1506	—	—
	$^2F_{7/2}$	2270	2269	—	2264
		2996	2984	—	—
		3402	3409	—	—
		—	—	—	—

[a]This work.
[b]Reference 39.
[c]Reference 47.

orders-of-magnitude lower concentration of Eu^{3+} and Pr^{3+} the fluorescence signal is comparable or higher than the ERS signal of Ce^{3+}.

Vibrational modes of the Y_2O_3 lattice also appeared in the Stokes spectrum. Of the 22 first-order Raman-active modes,[12,38,39] 15 were observed. All other experimental parameters remaining constant, the relative intensities of the lattice phonon modes did not change appreciably with excitation frequency. The intensity of any of the prominent phonon modes may, therefore, be used as a reference to compare the intensities of the ER transitions observed under different experimental conditions.

B. Resonance enhancement

It follows from the theoretical expression for the Raman-scattering amplitude,[40,41]

$$(\alpha_{\rho\sigma})_{fg} = -\frac{1}{hc}\sum_i \left[\frac{\langle f|\mathbf{e}_s\cdot\mathbf{r}|i\rangle\langle i|\mathbf{e}\cdot\mathbf{r}|g\rangle}{\nu_{gi}-\nu-i\Gamma_i} + \frac{\langle f|\mathbf{e}\cdot\mathbf{r}|i\rangle\langle i|\mathbf{e}_s\cdot\mathbf{r}|g\rangle}{\nu_{gi}+\nu_s-i\Gamma_i} \right], \quad (1)$$

that if the excitation frequency is resonant ($\nu \rightarrow \nu_i$) with any real intermediate state of the system, a large enhancement in the Raman signal is expected. In Eq. (1), σ and ρ are the polarization and ν and ν_s are the energies (in cm^{-1}) of the incident and scattered light, respectively; $|g\rangle$, $|f\rangle$, and $|i\rangle$ are the ground, final, and intermediate states of the ion, respectively; Γ_i is the half width at half maximum (HWHM) in cm^{-1} of the intermediate state $|i\rangle$; and ν_{gi} is the ground-to-intermediate state energy separation in cm^{-1}. The summation extends over all the intermediate states of the active ion. The theoretical prediction has been experimentally verified in several systems.[1,9,11,13,24] For a sample with more than one active site, resonant excitation of one of the sites would lead to a preferential enhancement of ER transitions belonging to that site compared to those of nonresonant sites. Resonance enhancement may therefore be used as a criterion to identify ER transitions within the states of a particular site.

Since the $4f \rightarrow 5d$ absorption spectra of the C_{3i} and C_2 sites are broad and overlapping, any laser frequency that resonantly excites the lowest $5d$ state of one of the centers would also be nearly resonant with that of the other. Even with this potential problem, the relative enhancement of the signal from the resonant site compared to that from the near-resonant site was nevertheless readily observed.

The 2270 and 2129 cm^{-1} Raman lines belonging to C_{3i} and C_2 sites, respectively, were used to illustrate this resonance enhancement. These lines had the largest intensities of the ER transitions with the smallest linewidths in their respective sites for all excitation frequencies. In addition, the 141-cm^{-1} energy separation between the two was small enough so that the response of the Raman system (frequency response, quantum efficiency of the photomultiplier tube, etc.) remained reasonably constant for the same laser excitation. Figures 3(a)–3(c) illustrate this

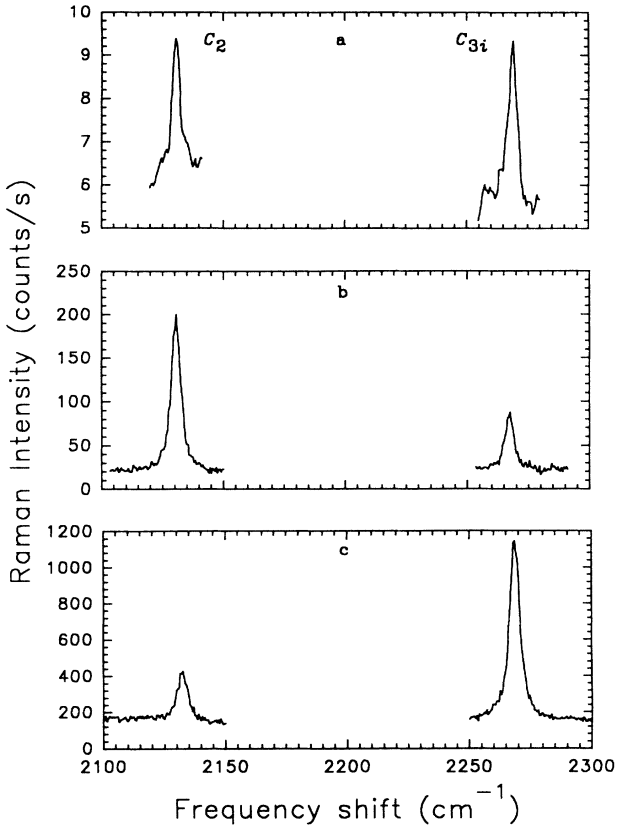

FIG. 3. Stokes ERS intensity of the 2129 cm^{-1} (C_2) and 2270 cm^{-1} (C_{3i}) lines for (a) nonresonant excitation at 632.8 nm, (b) resonant excitation of the lowest $5d$ state of the C_2 site at 457.9 nm, and (c) resonant excitation of the lowest C_{3i} $5d$ level at 514.5 nm. The change in the relative intensities of the two lines for different excitations illustrates the resonant enhancement effect and its site selectivity. The differences in absolute intensity (counts/s) in the three spectra are due to the differences in the incident laser power at the three excitation wavelengths.

resonance enhancement effect. We have observed this enhancement for all ER transitions listed in Table I.

For a more quantitative estimate of the enhancement factor, ERS intensities for resonant and nonresonant excitation were normalized by the intensity of the 379-cm^{-1} $A_g + T_g$ mode[38] of Y_2O_3 and compared. The normalization corrects for differences between experimental parameters (e.g., laser power, frequency response, etc.) and variations resulting from the ν^4-type scattering dependence and enables one to estimate the relative enhancement. Resonance enhancement factors of two orders of magnitude in both the C_{3i} and C_2 sites were observed.

The resonance enhancement also enabled the detection and identification of weak transitions. For example, the 2793-cm^{-1} ER transition of the C_2 site was not observed for 514.5 nm excitation, but could be studied even with 5-times weaker but resonant 457.9 nm excitation.

C. Measurement of the scattering cross section

We have estimated the differential scattering cross section of ER transitions by comparing their intensities to

that of the well-characterized and accurately measured 992-cm^{-1} vibrational Raman transition in benzene for the nonresonant 632.8 nm excitation. The differential scattering cross section for the 379-cm^{-1} $T_g + A_g$ phonon mode of Y_2O_3 is given in terms of that of benzene by the relation

$$\left[\frac{d\sigma}{d\Omega}\right]_Y = \Omega_{BY}\frac{I_Y N_B L_B}{I_B N_Y L_Y}\left[\frac{d\sigma}{d\Omega}\right]_B , \quad (2)$$

where the subscripts Y and B denote Y_2O_3 and benzene, respectively, Ω_{BY} is a correction term that takes into account the different solid angles of collected scattered light due to different sample geometry and the different indices of refraction for the two samples, I is the intensity of the scattered light, N is the number of ions or molecules per cm^3, and L is the effective length of the sample from which scattered light is collected and made to enter the entrance slit of the spectrometer.

Using Eq. (2), measured intensities and the known value of 8.0×10^{-30} $cm^2\,sr^{-1}$ per ion for the reference transition in benzene for 632.8 nm excitation,[42] the differential scattering cross section for the 379-cm^{-1} $T_g + A_g$ mode of Y_2O_3 was determined to be 5.1×10^{-30} $cm^2\,sr^{-1}$ per molecule. Since we have normalized the intensities of ER transitions relative to that of this phonon mode, the cross sections for these transitions may, therefore, be determined from the relative intensities.

The differential scattering cross section for the 2129-cm^{-1} ER transition of Ce^{3+} in the C_2 site was thus estimated to be 2.2×10^{-30} $cm^2\,sr^{-1}$ per ion and that of the 2270-cm^{-1} transition of the C_{3i} site to be 8.8×10^{-30} $cm^2\,sr^{-1}$ per ion. These lines correspond to transitions to the first excited state of the $^2F_{7/2}$ manifold of their respective sites. The cross-section values are comparable to 3.25×10^{-30} $cm^2\,sr^{-1}$ per ion obtained for the same transition in Ce^{3+}:$LuPO_4$.[10]

V. DISCUSSION

A. Energy-level structure of the $4f^1$ configuration

The ground state of the free Ce^{3+} ion is split by the spin-orbit interaction into the $^2F_{5/2}$ and $^2F_{7/2}$ multiplets.[43] These manifolds are further split by the crystal fields of C_{3i} and C_2 local symmetries of the Y_2O_3 host. Both the crystal fields split the $^2F_{5/2}$ manifold into three and the $^2F_{7/2}$ into four Kramer doublets. We have identified all three levels of the $^2F_{5/2}$ manifold and three out of four levels belonging to the $^2F_{7/2}$ manifold of Ce^{3+} in the C_{3i} site. The position of the first excited level of the $^2F_{5/2}$ manifold and three levels of the $^2F_{7/2}$ manifold of the C_2 site were also determined.

A weak, broad line appears at 1220 cm^{-1} in the ER spectra taken with 457.9, 476.5, and 488 nm excitations. The feature is masked by strong Eu fluorescence in the spectrum of Fig. 2. The linewidth of the transition is $\sim$50 cm^{-1} at 92 K, and its strength exhibits the same resonance enhancement behavior that is observed for ER transitions within the states of the C_2 site. No electronic energy level exists within 90 cm^{-1} of that energy.[28] However, when the energy of the observed $^2F_{5/2}$ level, 666 cm^{-1}, is added to the energy, 552 cm^{-1}, of the second highest-frequency optical phonon of the host lattice, the total energy $(666+552)=1218$ cm^{-1} corresponds to that of the observed transition. We therefore tentatively ascribe the 1220 cm^{-1} line to a vibroelectronic Raman transition which involves simultaneous change of both the electronic and vibrational quantum numbers. The vibroelectronic Raman effect was experimentally observed in rare-earth ion-doped crystals and a detailed theory was developed by Kane-Maguire and Köningstein.[44]

B. Cross-section calculation

A second-order perturbation-theoretical description of the ERS process will be used to obtain a semiquantitative understanding of the experimental results. According to this theory, the differential scattering cross section for an ER transition from a ground (initial) state $|g\rangle$ to a final state $|f\rangle$ is given by[40,41]

$$\frac{d\sigma}{d\Omega} = \Lambda_{SI}\eta_S^2\eta_I^2\frac{(2\pi)^4 e^4 \nu\nu_s^3}{(4\pi\varepsilon_0)^2}|(\alpha_{\rho\sigma})_{fg}|^2 , \quad (3)$$

where the subscripts S and I refer to the scattered and incident photons, respectively, $\eta=\frac{1}{3}(n^2+2)$ is the local field correction,[45] and ε_0 is the permittivity of free space. The factor Λ_{SI} depends on the geometric arrangement of the experiment and for the geometry used in this experiment is given by[46]

$$\Lambda_{SI} = \frac{16}{|1+n_S|^2|1+n_I|^2} , \quad (4)$$

where n_S and n_I are the refractive indices of the crystal for scattered and incident radiations, respectively. $(\alpha_{\rho\sigma})_{fg}$ is the scattering amplitude defined in Eq. (1). Since even for a moderately complex ion all the states are not well known, approximation schemes are necessary to evaluate the sum in Eq. (1) and extract a value for the cross section.

An order-of-magnitude estimate of the size of the *resonantly enhanced* intra-$4f$ ERS differential scattering cross section may, however, be made by assuming that the lowest-$5d$ resonant intermediate state is the only state that contributes appreciably to the cross section so that the sum in Eq. (1) is replaced by a single term. Under this assumption Eq. (3) reduces to

$$\frac{d\sigma}{d\Omega} = \Lambda_{SI}\eta_S^2\eta_I^2\frac{(2\pi)^2\nu\nu_s^3}{(4\pi\varepsilon_0)^2\hbar^2c^2}\frac{|\mu_{fi}\mu_{ig}|^2}{\Gamma_i^2} , \quad (5)$$

where μ_{fi} and μ_{ig} are the electric-dipole matrix elements connecting the final state to the resonant intermediate state and the ground state to the intermediate state, respectively. For this estimate we take $\mu_{fi}\sim\mu_{ig}\sim1\times10^{-18}$ esu, typical of $4f\rightarrow5d$ interconfigurational moments;[47] ν is 19 436 cm^{-1} and ν_s is 17 166 cm^{-1}, corresponding to a frequency shift of 2270 cm^{-1} (energy of the lowest level of the $^2F_{7/2}$ manifold in the C_{3i} site); the index of refraction of Y_2O_3 is 1.94 at 19 436 cm^{-1} and 1.93 at 17 166

cm^{-1};[36] and the linewidth of the lowest $5d$ level is approximately 1200 cm^{-1} from diffuse reflection spectra.[30] Substituting these parameters into Eq. (5), the resonant differential scattering cross section for the 2270-cm^{-1} ER transition of Ce^{3+} in the C_{3i} site of Y_2O_3 is found to be 8.0×10^{-27} $cm^2\,sr^{-1}\,ion^{-1}$. The effect of absorption of the laser excitation near resonance is minimized in the backscattering geometry used in this study and has been neglected. The experimental value of the differential scattering cross section for this transition determined from its normalized intensity, resonance enhancement, and the cross section for the 379-cm^{-1} T_g+A_g phonon mode of Y_2O_3 (5.1×10^{-30} $cm^2\,sr^{-1}$ per molecule) is 1.2×10^{-27} $cm^2\,sr^{-1}$ per ion, in reasonable agreement with the theoretical estimate.

For *nonresonant excitation* the sum in Eq. (1) was evaluated using the approximation scheme developed by Axe for two-photon processes,[48] following the Judd-Ofelt formalism for intra-$4f$ induced-electric-dipole one-photon transitions in R^{3+} ions.[49,50] The application of the formalism to the present problem is somewhat involved but standard and will be detailed elsewhere.[51] Calculation of the cross section using this formalism requires knowledge of correct crystal-field wave functions for the initial and final states. These are not readily available for Ce^{3+} in C_{3i} and C_2 sites of Y_2O_3. However, for an order-of-magnitude estimate, wave functions for a crystal field of higher symmetry may be used. The crystal field of the C_2 site thus may be approximated by that of a cube with eight oxygen ions at the corners and Ce^{3+} at the body center. This approximation seems to provide a reasonable explanation of the principal features of the energy-level structure.[30] The wave functions of this cubal coordination were tabulated by Manthey.[52] We have used these wave functions in estimating the nonresonant differential scattering cross section for the 2129-cm^{-1} ER transition. Other relevant parameters for this transition are $\nu=15\,803$ cm^{-1}, $\nu_s=13\,674$ cm^{-1}, $\nu_c(5d)=35\,000$ cm^{-1}, and $\langle R_{5d}|r|R_{4f}\rangle=3.91\times10^{-9}$ cm.[53] The estimated value of the cross section is 1.2×10^{-30} $cm^2\,sr^{-1}$ per ion, which is in good agreement with the experimental value of 2.2×10^{-30} $cm^2\,sr^{-1}$ per ion.

VI. CONCLUSION

Electronic-Raman scattering was used to identify and determine the energies of six of the seven Kramer doublets of the $4f$ ground configuration of Ce^{3+} in the C_{3i} site of Y_2O_3. Five of the seven $4f$ levels of Ce^{3+} in the C_2 site were also identified.

The differential scattering cross sections for nonresonant ER transitions from the ground state to the lowest level of the $^2F_{7/2}$ manifold of both C_{3i} and C_2 sites were measured to be 8.8×10^{-30} and 2.2×10^{-30} $cm^2\,sr^{-1}$ per ion, respectively. Estimates based on a second-order perturbation-theoretical model are in reasonable agreement with the experimental results.

For resonant excitation, over two-orders-of-magnitude enhancement in ER transition strength was observed. Selective excitation of a resonant intermediate state of a particular site led to enhancement of transitions within that site as compared to that of the other site, making the technique site selective. This site selectivity of resonant ER transitions facilitated the determination of the low-lying energy-level structure of Ce^{3+} in both C_{3i} and C_2 sites. The resonant ERS technique is thus expected to be a powerful spectroscopic tool in the study of low-lying energy levels of impurity ions in solids and in identifying the sites to which these belong when several inequivalent sites are present.

ACKNOWLEDGMENTS

The authors gratefully acknowledge S. L. Dole and C. D. Greskovich of General Electric Research and Development Center for fabricating the samples and T. R. Hart of the Department of Physics and Engineering Physics at Stevens Institute of Technology for making the experimental facilities available for this study.

*Present address: Department of Physics, Rensselaer Polytechnic Institute, Troy, New York 12180.

†Present address: Department of Earth Science, University of Oxford, Oxford, OX1 3PR, U.K.

[1]For an excellent review of the ERS technique and pertinent literature up until 1982, see R. J. H. Clark and T. J. Dines, in *Advances in Infrared and Raman Spectroscopy,* edited by R. J. H. Clark and R. E. Hester (Heyden, London, 1982), Vol. 9, pp. 283–360.

[2]J. T. Hougen and S. Singh, Phys. Rev. Lett. **10**, 406 (1963).

[3]J. T. Hougen and S. Singh, Proc. R. Soc. London A **227**, 193 (1964).

[4]R. J. Elliott and R. Loudon, Phys. Lett. **3**, 189 (1963).

[5]J. Y. H. Chau, J. Chem. Phys. **44**, 1708 (1966).

[6]J. A. Köningstein and O. S. Mortensen, in *Light Scattering Spectra of Solids,* edited by G. W. Wright (Springer-Verlag, New York, 1969), pp. 239–243.

[7]J. A. Köningstein and O. S. Mortensen, in *The Raman Effect,* Vol. 2, edited by A. Anderson (Dekker, New York, 1971), pp. 519–542.

[8]J. E. Smith, Jr., F. Holtzberg, M. I. Nathan, and J. C. Tsang, in *Light Scattering in Solids,* edited by M. Balkanski, R. C. C. Leite, and S. P. S. Porto (Flammarion, Paris, 1976), pp. 313–316.

[9]G. W. Williams, P. C. Becker, J. G. Conway, N. Edelstein, L. A. Boatner, and M. M. Abraham, Phys. Rev. B **40**, 4132 (1989).

[10]G. M. Williams, N. Edelstein, L. A. Boatner, and M. M. Abraham, Phys. Rev. B **40**, 4143 (1989).

[11]D. Piehler and N. Edelstein, Phys. Rev. A **41**, 6406 (1990).

[12]G. Schaack and J. A. Köningstein, J. Opt. Soc. Am. **60**, 1110 (1970).

[13]P. C. Becker, G. M. Williams, R. E. Russo, N. Edelstein, J. A. Köningstein, L. A. Boatner, and M. M. Abraham, Opt. Lett.

11, 282 (1986).
[14]I. Mörke, E. Kaldis, and P. Wachter, Phys. Rev. B **33**, 3392 (1986).
[15]E. Zirngiebl, S. Blumenröder, and G. Güntherodt, J. Magn. Magn. Mater. **47&48**, 72 (1982).
[16]von H. D. Amberger, G. G. Rosenbauer, and R. D. Fischer, Mol. Phys. **32**, 1291 (1976).
[17]D. Piehler, J. Opt. Soc. Am. **8**, 1889 (1991).
[18]K. P. Traar, Phys. Rev. B **35**, 3111 (1987).
[19]K. Leiteritz and G. Schaack, J. Raman Spectrosc. **10**, 36 (1981).
[20]M. L. Shand, J. Appl. Phys. **52**, 1470 (1981).
[21]P. Myslynski and J. A. Köningstein, Chem. Phys. **114**, 137 (1987).
[22]J. B. Gruber, R. D. Chirico, and E. F. Westrum, Jr., J. Chem. Phys. **76**, 4600 (1982).
[23]P. C. Becker, N. Edelstein, G. W. Williams, J. J. Bucher, R. E. Russo, J. A. Köningstein, L. A. Boatner, and M. M. Abraham, Phys. Rev. B **31**, 8102 (1985).
[24]G. M. Williams, P. C. Becker, N. Edelstein, L. A. Boatner, and M. M. Abraham, Phys. Rev. B **40**, 1288 (1989).
[25]J. A. Köningstein, Phys. Rev. **174**, 477 (1968).
[26]S. Guha, Phys. Rev. B **23**, 6790 (1981).
[27]G. Blasse and A. Bril, J. Chem. Phys. **47**, 5139 (1967).
[28]N. C. Chang, J. B. Gruber, R. P. Leavitt, and C. A. Morrison, J. Chem. Phys. **76**, 3877 (1982).
[29]F. A. DiBianca, J. J. Georges, D. A. Cusano, and C. D. Greskovich, U.S. Patent 4,525,628, 25 June 1985.
[30]G. A. Slack, S. L. Dole, V. G. Tsoukala, and G. S. Nolas, J. Opt. Soc. Am. B **11**, 961 (1994).
[31]R. W. G. Wyckoff, *Crystal Structures* (Wiley, New York, 1960), Vol. II.
[32]M. Faucher and J. Pennetier, Acta. Crystallogr. B **36**, 3209 (1980).
[33]A. G. Schäfer, Phys. Kondens. Mater. **9**, 359 (1969).
[34]H. Forest and G. Ban, J. Electrochem. Soc. **118**, 1999 (1971).
[35]H. T. Hintzen and H. M. Van Noort, J. Phys. Chem. Solids **49**, 873 (1988).
[36]Y. Nigara, Jpn. J. Appl. Phys. **7**, 404 (1968).
[37]L. Lyu and D. S. Hamilton, J. Lumin. **48&49**, 251 (1991).
[38]J. Gouteron, J. Zarembowitch, and A. Lejus, Acad. Sci. Ser. C **283**, 243 (1979).
[39]W. B. White and V. G. Keramidas, Spectrosc. Acta A **28**, 501 (1972).
[40]R. Loudon, *The Quantum Theory of Light* (Clarendon, Oxford, 1983), p. 314.
[41]O. S. Mortensen and J. A. Köningstein, J. Chem. Phys. **48**, 3971 (1968).
[42]Y. Kato and H. Takuma, J. Chem. Phys. **54**, 5398 (1971).
[43]R. J. Lang, Can. J. Res. A **14**, 127 (1936).
[44]C. Kane-Maguire and J. A. Köningstein, J. Chem. Phys. **59**, 1899 (1973).
[45]D. L. Dexter, in *Advances in Research and Applications, Solid State Physics* Vol. 6, edited by F. Seitz and D. Turnbull (Academic, New York, 1958), p. 363.
[46]W. Hayes and R. Loudon, *Scattering of Light by Crystals* (Wiley, New York, 1978), p. 190.
[47]M. A. Kramer and R. W. Boyd, Phys. Rev. B **23**, 986 (1981).
[48]J. D. Axe, Jr., Phys. Rev. **136**, A42 (1964).
[49]B. R. Judd, Phys. Rev. **127**, 750 (1962).
[50]G. S. Ofelt, J. Chem. Phys. **37**, 511 (1962).
[51]G. S. Nolas, Ph.D. thesis, Stevens Institute of Technology, 1994.
[52]W. J. Manthey, Phys. Rev. B **8**, 4086 (1973).
[53]S. K. Gayen, D. S. Hamilton, and R. H. Bartram, Phys. Rev. B **34**, 7517 (1986).